Materials and Structures (2017) 50:93
DOI 10.1617/s11527-016-0960-z

Calcium sulfoaluminate cement pastes from industrial wastes: effect of hemihydrate content

M. Gallardo-Heredia · J. M. Almanza-Robles · R. X. Magallanes-Rivera · D. A. Cortes-Hernández · J. C. Escobedo-Bocardo · U. Avila-López

Received: 9 June 2016 / Accepted: 15 October 2016 / Published online: 24 October 2016

Abstract In this work, the effects of the variation of hemihydrate and the water/cement ratio were evaluated on the compressive strength and reaction mechanisms in pastes of calcium sulfoaluminate cement (CSA cement) prepared from industrial wastes as fluorgypsum, aluminum dross and fly ash. Based on stoichiometric calculations and the chemical compositions of the raw materials, CSA clinker, with low content of belite was synthesized at 1250 °C for 4 h. In general, compressive strength of ~40 MPa were reached after 360 days of curing: strength increased as water/cement reduced. Ettringite and gypsum were the main hydration products forming dense microstructures of intertwined crystals; while gehlenite and spinel formed in the CSA clinker did not present any hydraulic behavior. The increment in the hemihydrate provoked lower setting times by an enhanced rate of ettringite formation; however, in some cases it was detected a decrease in strength after 90 days due to the delayed formation of this phase. It was observed the formation of two main exothermic manifestations by isothermal calorimetric tests corresponding to gypsum and ettringite formation; however, an overlap of both processes was noted as the temperature was increased.

Keywords Calcium sulfoaluminate · Ettringite · Compressive strength · Calorimetry · By-products · Hemihydrate

M. Gallardo-Heredia (✉) · J. M. Almanza-Robles · D. A. Cortes-Hernández · J. C. Escobedo-Bocardo · U. Avila-López
Centro de Investigación y de Estudios Avanzados del IPN Unidad Saltillo, CP 25900 Ramos Arizpe, COAH, Mexico
e-mail: marisol.gallardo@uadec.edu.mx

Present Address:
M. Gallardo-Heredia · R. X. Magallanes-Rivera
Universidad Autónoma de Coahuila – Facultad de Ingeniería, Blvd. Fundadores Km 13, Ciudad Universitaria, CP 25354 Arteaga, COAH, Mexico

1 Introduction

The fabrication of Portland cement involves temperatures near 1450 °C and decarbonation processes that represent about 10 % of CO_2 liberation worldwide annually [1]. This establishes the necessity for the development of eco-friendly cements capable of reduce such emissions by partial or total replacement of Portland cement [2, 3]. On the other hand, technological innovations that allow an efficient management of industrial wastes through recycling and reuse, could contribute to the preservation of the planet's natural resources and reduction in the energy requirements for the synthesis of hydraulic cements [4, 5].

The manufacture of calcium sulfoaluminate cements (CSA) emerges as a real alternative to the aforementioned, as can be synthesized at relative low

temperatures with reduced CO_2 emissions [6]. They have an adequate development of mechanical properties and are composed mainly by CaO, Al_2O_3 and SO_3 [7–9], that can be obtained from industrial wastes and byproducts such as fly ash, aluminum dross and fluorgypsum [10–16]. According the European List of Waste (MAM, BOE 19/2/2014, Spain [17]) these materials are classified as non-hazardous (fly ash) and potentially hazardous residues (fluorgypsum and aluminum slag).

A typical CSA clinker consists predominantly of calcium sulfoaluminate and belite with lower percentages of ferrite, mayenite, periclase, perovskite, gehlenite and calcium aluminate [18]. The synthesis of the reactive phases is strongly dependent on starting materials and temperature; however, depending on the minor phases, a complex synergy of reactions could lead to very different hydration mechanisms and structuration of products [19, 20]. In the hydration of CSA cements, the main product is ettringite which is formed by dissolution of the calcium sulfoaluminate and precipitation of ettringite, aluminum hydroxide and sometimes monosulphate [20]; once the CSA begins to consume, the ettringite formation can continue in the presence of gypsum [21, 22]:

$$C_4A_3\overline{S} + 2C\overline{S}H_2 + H_{34} \rightarrow C_3A(C\overline{S})_3H_{32} + 2AH_3 \quad (1)$$

Nevertheless, fast setting and expansion may originate if calcium sulfate is added in excess (20–30 %) [18]. The formation of ettringite at early stages of hydration contributes to the development of mechanical properties; however, the development of this phase at later stages, which is known as delayed ettringite formation (DEF), can be unfavorable due to expansive processes. The DEF is often attributed to an excessive amount of sulfate [24, 25, 42].

In diverse studies concerning the hydration of CSA, it was concluded that the rate of ettringite formation is strongly dependent on the type and quantity of the calcium sulfate added: increasing the amount of hemihydrate, an expansion occurs by crystal growth around the cement grains; while in pastes with anhydrite, there is no expansion because the crystal growth occurs in the solution but the mechanical properties are poor since anhydrite dissolves very slowly [7, 24, 26, 27]. The latter is of great importance as dimensional stability and strength development are major factors in the durability, and on the other hand, hemihydrate manufacture requires less energy than the artificial synthesis of anhydrite and leads to a better performance, hence the importance of studies involving the hydration mechanisms of CSA cements with hemihydrate.

In this work, the effects of the composition of the binder, in terms of the content of commercial β-hemihydrate, and the water/cement ratio were studied on the development of mechanical properties of CSA pastes cured from 1 to 360 days. Studies based on isothermal conduction calorimetry and XRD were carried out to establish the effects that directly influences the development of microstructures, the formation of hydration products and dimensional stability in CSA cement pastes synthesized from industrial wastes.

2 Experimental

Table 1 shows the chemical composition of the raw materials used: fly ash (FA), aluminum slag (AS) and fluorgypsum (FG), analyzed by semiquantitative spectrometric method (XRF) with dispersion wavelength (BRUKER, Model S4 PIONEER). The fluorgypsum did not show fluorine in its chemical composition that could affect the formation of calcium aluminate phases [25], consistent with other reports for this material (Escalante-Garcia et al. 2008). The AS were ball milled for 2 h in a stainless steel container (5 L) for separation of Al^0 residues to a particle size of <106 μm.

Table 1 Chemical composition in main oxides of raw materials by XRF (wt%)

Oxide	AS	FA	FG
Na_2O	2.5	–	–
MgO	5.0	1.4	–
Al_2O_3	63.2	24.8	–
SiO_2	11.7	59.5	0.1
SO_3	0.8	–	56.3
Cl_2	4.6	–	–
K_2O	2.2	1.7	–
CaO	7.3	4.8	43.2
TiO_2	0.9	1.7	–
MnO	0.5	–	–
Fe_2O_3	1.2	6.1	–

AS aluminum slag, *FA* fly ash, *FG* fluorgypsum, *CSA clinker* AS 45.53 wt%; FA 0.64 wt%; FG 12.82 wt%; $CaCO_3$ 41 wt%, *Blaine* 3800 cm^2/g, Density 2.9 g/cm^3

The AS was blended with the FG and FA in adequate proportions and homogenized in plastic containers for up to 4 h before the synthesis of the CSA clinker. Taking into account the data in Table 1 and based on stoichiometric mass balances (regardless impurities or inert phases in raw materials), the starting proportioning was adjusted with $CaCO_3$ (industrial grade, 97 % purity) for the clinkerization. The adjustment was carried out so that the percentage of CSA was 80 and 20 wt% of Ca_2SiO_4 (C_2S), as typical CSA clinkers [28]. Samples of 2 cm of diameter were prepared by uniaxial pressing at 44 MPa and were calcined in Al_2O_3 containers at 1250 °C for 4 h in a Thermolyne 46,200 furnace with a heating rate of 10 °C/min. The clinker was cooled inside the oven until it can be manipulated. Clinker formation of CSA was confirmed by XRD as will be seen in Sect. 3.

2.1 Specimens preparation

The clinker was ball milled in an Al_2O_3 container to a Blaine fineness of 380 m^2/kg. It was subsequently mixed with 15, 20 or 25 wt% of commercial β-$CaSO_4 \cdot ½H_2O$ (Yesera Monterrey) in a mechanical homogenizer with Al_2O_3 balls during 2 h. Pastes were prepared according the procedure described in the Mexican standard (NMX-C-085 [29]) with two different water/cement (*w*/*c*) ratios (0.4 or 0.5). The pastes were casted into cubic molds of 25 mm and vibrated for 60 s. The molds were covered with plastic sheets and placed in isothermal conditions (20 °C) for 24 h; subsequently, the cubes were demolded and placed in containers with water for up to 360 days. The volume ratio solid:water in the containers was 1:4. The identification for each system will be of three digits (e.g. 415); the first will refer to the *w*/*c* ratio and the last two to the hemihydrate percentage.

2.2 Characterization

The apparent porosity (% AP) of selected systems was evaluated according international standard (ASTM-C-20 [30]), which indicates measurements of the samples in saturated, suspended and dry weight. Additionally, pH measurements were performed to establish potential leaching using an ORION pH-meter model 250A. Based on the Forrester design [31], isothermal conduction calorimetry was used to register the rate of heat evolution: 15 g of CSA cement with 15, 20 or 25 wt% of hemihydrate at 20, 30 and 40 °C were set as study, while the *w*/*c* ratio was fixed at 0.4 or 0.5. The setting times were determined by Vicat needle (ASTM-C-191 [32]) and compressive strength (CS) tests were performed after 1, 3, 7, 14, 28, 90, 180, 270 and 360 days under the procedure established in the Mexican standard (NMX-C-061 [33]).

After the CS assays, fragments of the collapsed cubes were immersed in methanol in order to stop the reactions. To identify the phases present at different ages of curing, the samples were grounded to <150 μm using a planetary mill (Retsch PM 400/2) and were further analyzed by XRD (X'Pert Phillips XPD): scanning range 7–80°2θ, step of 0.03°2θ and incidence time of 3 s/step. For the study of the microstructures, fracture surfaces of the samples were carbon-coated and observed under SEM (Phillips XL30 ESEM) using the secondary electron technique and performing EDS X-ray microanalysis on selected areas.

3 Results and discussion

Figure 1 shows the XRD pattern of the synthesized clinker at 1250 °C. Reflections corresponding to the formation of calcium sulfoluminate ($Ca_4Al_6O_{12}(SO_4)$-ICSD# 28480) are observed throughout the figure; similarly, gehlenite ($Ca_2Al_2SiO_7$-ICSD#39921), calcium aluminate ($CaAl_2O_4$-ICSD#260), mayenite ($Ca_{12}Al_{14}O_{33}$- ICSD#6287), pleochroite ($Ca_{20}Al_{26}Mg_3Si_3O_{68}$-ICSD#25353) and spinel ($MgAl_2O_4$-ICSD#79000) are also observed. Peaks of belite (Ca_2SiO_4-ICSD#963) are observed in Fig. 1; however, according a semi-quantitative phase analysis performed (XPowder), this phase was obtained in a lower percentage than was intended (Sect. 2) due to the thermodynamic stability of the gehlenite and spinel [24]. The semi-quantitative analysis takes in consideration the intensity of the peaks and it showed 60 wt% calcium sulfoluminate, 6 wt% belite, 28 wt% gehlenite and 6 wt% of remaining phases. Despite the MgO present in the AS, no periclase was observed in the clinker and could be expected as in the form of spinel from the starting material. The presence of high contents of gehlenite may be due to sulfur losses on the synthesis, as $CaSO_4$ decomposition could be present at the temperature of clinkerization [18]. However, the

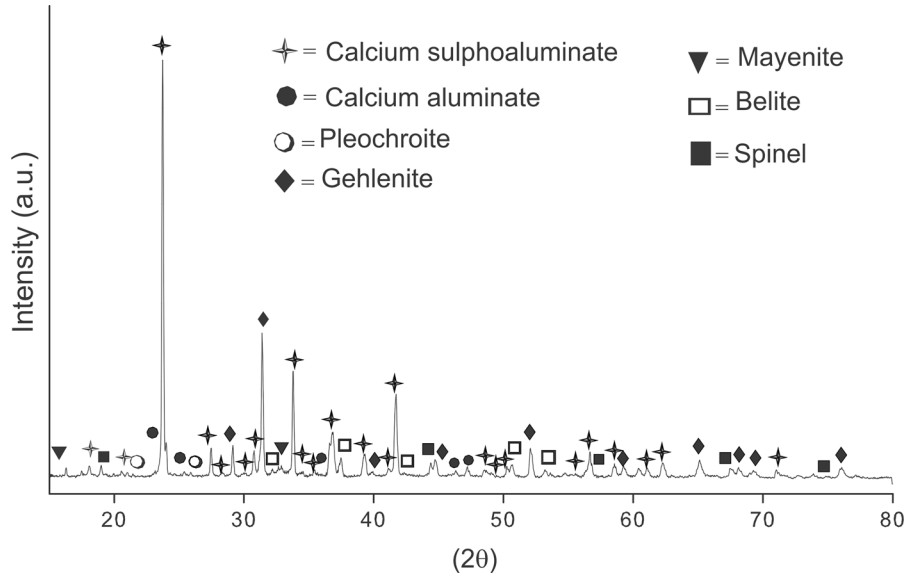

Fig. 1 XRD pattern of the synthesized clinker at 1250 °C for 4 h

calcium sulfoaluminate and the secondary phases observed are comparable to other works on CSA synthesized at similar temperatures [10–16, 18].

3.1 Time of setting

Table 2 shows the setting times for different systems; it can be observed that higher *w/c* ratios provoked higher setting times. In the other hand, systems 420 and 520 (20 wt% of $CaSO_4 \cdot ½H_2O$) exhibited lower setting times than pastes with 15 wt% hemihydrate. This behavior could be attributed to a higher concentration of Ca^{2+} and SO_4^{2-} ions provoking gypsum formation at a higher rate than pastes with lower content of hemihydrate. The system 525 presented initial and final setting of 23 and 40 min respectively, lower than systems 515 and 520, indicating that the reactions for crystals formation are faster in the first case due to a higher amount of $CaSO_4 \cdot ½H_2O$.

From the results of Table 2, it can be noted that the setting times of CSA cements are very short when compared with Portland cement, which has a permissible range of 45 and 375 min for initial and final setting times, respectively (ASTM-C-150 [34]), typically delayed by an initial formation of a C-S-H layer preventing dissolution [35]. In contrast, in the mechanisms of CSA cement reactions, hydration is carried out at a higher rate by the presence of $CaSO_4 \cdot ½H_2O$ acting as an activator for ettringite precipitation.

3.2 Compressive strength

The CS results of the studied systems are shown in Table 3 as an average of 4 samples; the standard deviation (SD) is also observed. In the system 415, an accelerated development of mechanical properties is observed in the first 72 h, reaching 49.4 MPa at 28 days; however, a continuous decrease was registered after that age. Strength loses in CSA cements are often attributed to the delayed formation of ettringite causing expansion and promoting microcracking in the matrix [24]. In this case, the drops after 90 days

Table 2 Times of setting of studied pastes cured at 20 °C

System	*w/c*	$CaSO_4 \cdot ½H_2O$ (wt%)	Initial (min)	Final (min)
415	0.4	15	36	58
515	0.5	15	43	65
420	0.4	20	28	46
520	0.5	20	39	60
525	0.5	25	23	40

Table 3 Compressive strength (MPa) of studied systems cured at 20 °C (SD ± 0.30–3.02)

System	Curing time (days)							
	1	3	7	14	28	90	180	360
415	17.9	43.2	45.0	47.3	49.3	43.3	40.8	34.3
515	14.9	19.0	22.1	24.7	23.2	19.8	19.0	20.6
420	18.0	24.6	42.6	43.3	43.6	37.7	46.7	36.8
520	16.6	21.3	26.7	26.5	26.3	26.9	25.8	20.9
425	23.6	30.2	32.8	28.6	32.6	34.3	36.1	39.0
525	17.9	19.6	18.3	21.7	24.8	21.1	23.8	27.3

could be attributed to the growth of ettringite originating internal stresses resulting in microstructural rearrangements. In the other hand, in the system 515 a maximum CS of 24.8 MPa was observed at 14 days; notably lower than the correspondent paste with $w/c = 0.4$ (415), and similarly, the CS is reduced from 28 days onwards. The strength loss in this case could be related to the porosity generated by a higher volume of mixing water not being filled by hydration products [36], as will be corroborated in the next section.

According Table 3, the system 420 exhibited an increase in CS from 1 to 28 days; after 90 days a decrease was observed, and a subsequent increment at 180 days was again detected. However, after that age a drop is again registered concluding with 36.0 MPa at 360 days. Similarly to system 415, the decrease in strength could be attributable to the delayed formation of ettringite, while the subsequent increase to the formation and growth of this phase within the microcracks promoting strength development [24]. Higher contents of gypsum increase the Ca^{2+} and SO_4^{2-} liberation promoting the formation and/or growth of late ettringite in small proportions. For the system 520, and similar to 515, an ascendant development was observed during the first 7 days onwards. Meanwhile, the paste 425 presented 32.8 MPa at 7 days; at 14 days a slight decrease was observed and then a gradual increment to 39.0 MPa at 360 days was registered. This behavior was similar to that observed in a Portland cement paste prepared and cured under the same conditions for comparison purposes [37]. The strength drop could be attributed to a higher amount of gypsum (25 %) accelerating the rate of ettringite formation, as will be discussed in Sect. 3.5. The system 525 presented a maximum CS of 27.3 MPa at 360 days; nevertheless, it surpassed the minimum permissible in specifications for hydraulic cements (ASTM-C-150 [32]; NMX-C-414 [38]).

3.3 Porosity

Figure 2 shows the results of the apparent porosity (AP) for selected systems. It is noted that the paste 525 registered a higher AP than the system 425; in agreement with the lower CS for this system (Table 3). In the paste 425, a decrease in the AP from 1 to 7 days was observed, while at 14 days the AP increased causing the drop in the CS discussed in the previous section. From 28 days onwards it was observed a continuous general reduction in the AP. These results, in addition with the CS observations, indicate that at initial stages of curing the porosity decrease as the structuration of hydration products fill the volume initially occupied by water. After 14 days, the formation and growth of hydrated phases generate an expansion of the material which leads to an increase in microcracks generated by dimensional changes, which subsequently are filled by the continuous densification processes from the ettringite growth.

3.4 pH of the curing medium

The pH measurements of the curing medium of the pastes are presented in Fig. 3. The initial pH of the curing water was 8.1; probably by the presence of mineral salts and impurities [37]. It was noted that

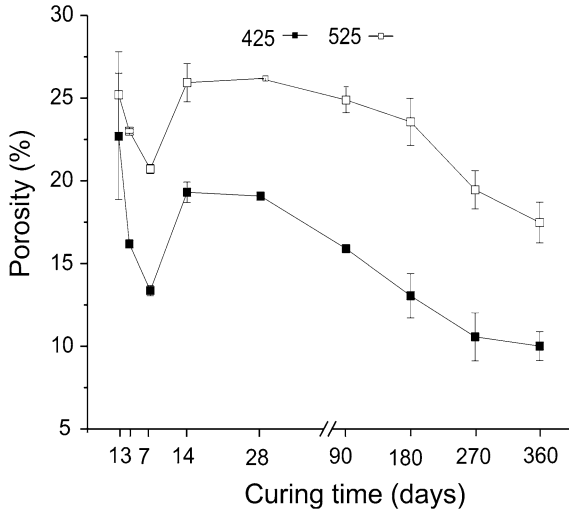

Fig. 2 Apparent porosity of systems 425 and 525 cured at 20 °C for 360 days

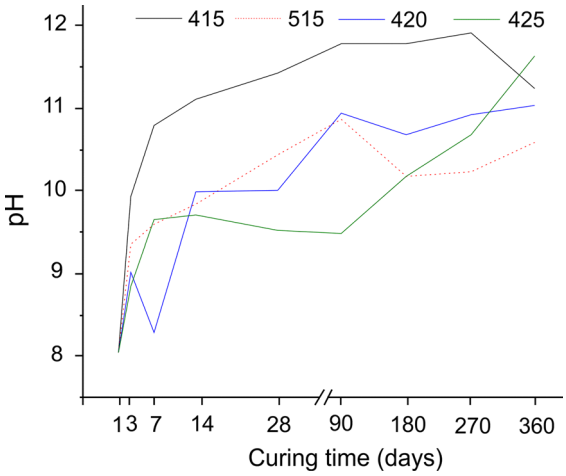

Fig. 3 pH of the curing water of studied systems cured at 20 °C

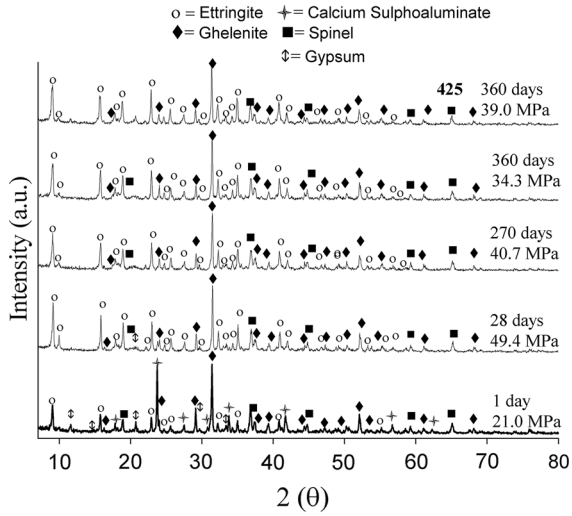

Fig. 4 XRD patterns of paste 415 (except where indicated) cured at 20 °C

systems with $w/c = 0.4$ presented higher pH than $w/c = 0.5$ (see dotted line) due to a higher concentration of solids in the paste that in contact with the aqueous medium promoted ion exchanges (release of Ca^{2+} and Al^{2+}) causing degradation of the ettringite and subsequent formation of external $Ca(OH)_2$ and $Al(OH)_3$ responsible for the increment in the pH [39, 40]. No evidence of gypsum decomposition was observed, as SO_4^{2-} in the curing medium was not detected by ICP analyses (not shown). In the pastes with higher content of gypsum (420 and 425) the initial increase in pH is lower than the system with less gypsum (415), probably by a higher structuration and impermeability caused by an increased formation of ettringite, which in turn decrease the ion exchange. Additionally, $Ca(OH)_2$ and $Al(OH)_3$ at the surface of the cubes could act as a barrier to ion migration, and the balance is reached at longer times as is shown in Fig. 3.

3.5 X-ray diffraction

It can be seen in Fig. 4 from the XRD results of paste 415, well-defined reflections after 24 h of the main hydration product ettringite ($Ca_6Al_2(SO_4)_3(OH)_{12}$-$26H_2O$-ICSD#16045); peaks of anhydrous CSA and gypsum ($CaSO_4{\cdot}2H_2O$-ICSD#2057) are also observed after 1 day, indicating that the CSA reactions are not completed, but hemihydrate and belite had been completely hydrated promoting the initial strength development. Ettringite reflections increased markedly after 28 days, where maximum strength was also observed, suggesting that the majority of this phase is formed. A semi-quantification of the ettringite (XPowder) was performed for the first 28 days in this system: 1 day-23.0 %, 7 days-42.0 %, 14 days-45.7 %, 28 days-47.2 %, suggesting that the CSA cement hydration is more significant during the first 7 days and gradually arises until 28 days, in coincidence with the observed strength development (Table 3). After 270 days, the intensity of the peaks of ettringite show a slight decrease, as was similarly observed for the reflections of the inert phases spinel and gehlenite, thus, the decrease in strength observed for this system at 270 days, was possibly derived from microstructural rearrangements, as XRD results do not suggest any significant changes in the formation of phases. Figure 4 shows the XRD pattern for the system 425 at 360 days of curing, where it is observed well defined peaks of ettringite and the absence of reflections of anhydrous CSA clinker or gypsum. This indicates that gypsum is actively involved in the early reactions, leading to the formation of ettringite, but without strength losses at later stages of curing (see Table 3).

3.6 Microstructures

Figures 5 and 6 show representative SEM results of the studied systems. In the micrograph of the paste 415 in Fig. 5, can be see that after 28 days it is present a compact morphology of elongated and intertwined crystals of ettringite conferring densification. It is also

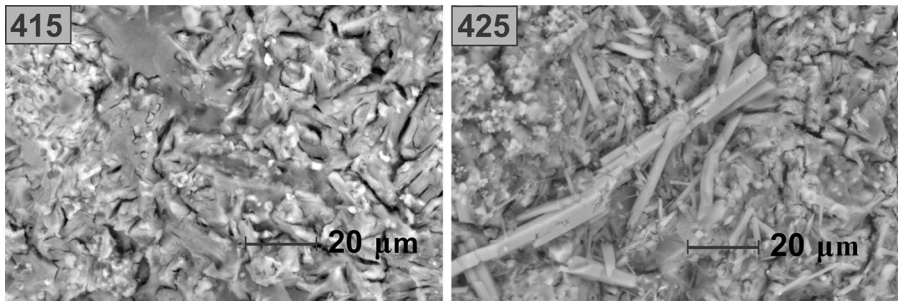

Fig. 5 SEM images of pastes 415 and 425 cured for 28 days at 20 °C

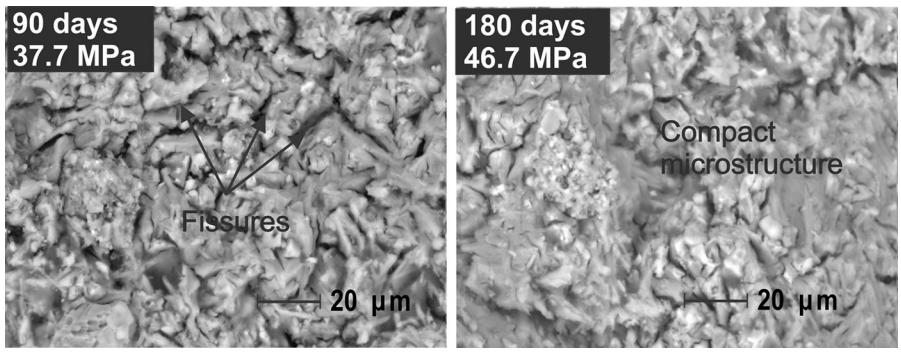

Fig. 6 SEM images of paste 420 cured at 20 °C

noted the presence of $Al(OH)_3$ as a result of the CSA cement reaction [27], corroborated by the absence of Ca and Al in EDS analyses performed in this zones [37]. Microcracks were observed in some specimens for the internal pressure of the ettringite formation; nevertheless, the CS reached the highest values at this age. In the image of the paste 425 in Fig. 5, is observed a more compacted and denser microstructure than the latter, possibly caused by the rapid hydration provoked from a higher amount of calcium sulfate. It is also noted large ettringite crystals on the surface of the matrix of hydration products; however, intertwined crystals of small size are also present densifying the microstructure.

Figure 6 shows micrographs of the paste 420, where it can be observed that after 90 days a microstructure with multiple microcracks resulted in the decrease in the CS (Sect. 3.2); however, after 180 days the cracks were diminished probably by the growth of new ettringite acting as a filler. However, cracking and consequent drop in strength was again observed at further ages probably to dimensional changes generated by the ettringite growth. The systems with lower *w/c* ratio resulted in smaller interlaced crystals and higher compaction than the pastes with $w/c = 0.5$, supporting the CS results.

3.7 Heat of hydration

Figure 7 shows the results of isothermal calorimetry for systems 415 and 515 hydrated at different temperatures. In the pastes at 20 °C it was observed that after the wetting of the powders an exothermic manifestation (peak 1) was presented almost immediately and lasting a few minutes indicating the start of the dissolution. After a very short induction period, the apparition of a peak 2 was observed, reaching a maximum rate of heat liberation (RHL) at 60 min of 5.3 and 7.5 W/kg for $w/c = 0.4$ and 0.5 respectively, which is attributable to the hydration of the hemihydrate provoking the setting of the pastes [41]; in parallel, the formation of calcium monosulphate from the CSA could also be carried out [42], nevertheless this phase was not detected by XRD nor ettringite during the first hours of hydration [37]. It is interesting to note that the maximum of peak 2 is within the range of the setting times (Table 2) when manipulation of the paste is possible.

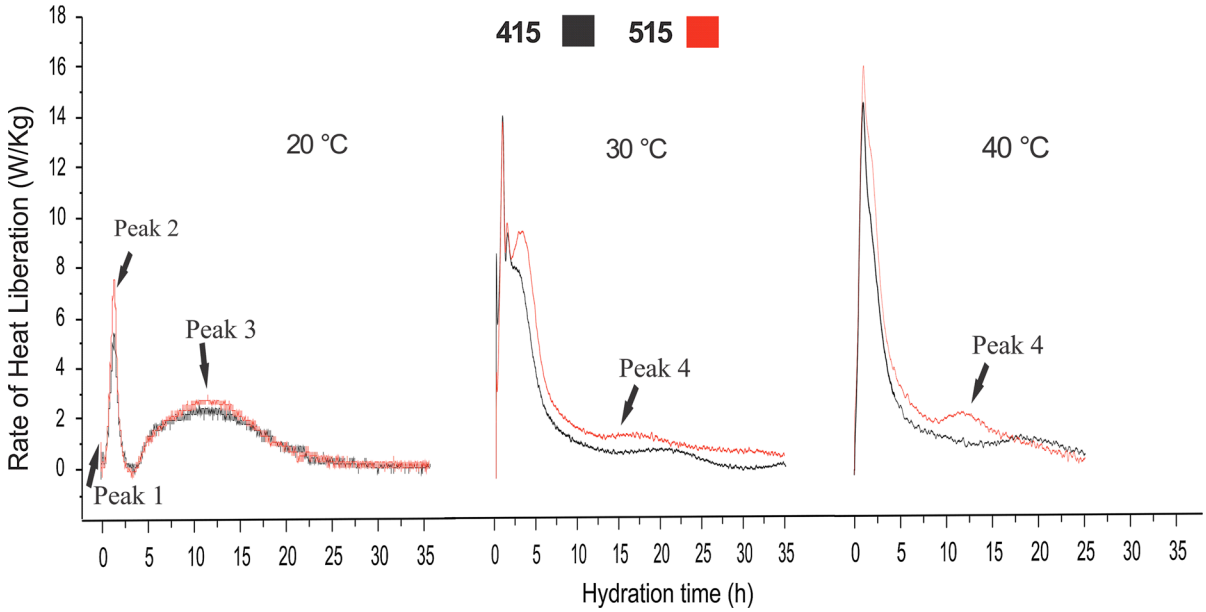

Fig. 7 Isothermal conduction calorimetry for the systems 415 and 515

A second period of induction can be seen in Fig. 7 at 20 °C with an onset at 4 h, diminishing the RHL almost to zero indicating a complete hemihydrate→gypsum conversion. From 4 to 22 h the RHL increases again with the formation of a peak 3, which is dependable on the initial CSA cement hydration forming ettringite. This peak reaches a maximum at 11 h and 2.6 W/kg for $w/c = 0.4$, and at 11.4 h and 2.8 W/kg for $w/c = 0.5$. It is interesting to note in Fig. 7 that peak 3 extends longer and is less intense than peak 2, suggesting a slow CSA cement→ettringite conversion. After 20 h a slowdown was observed in the RHL with a marked tendency to zero, indicating that the reactions are decelerating and will be completed until all reactants are consumed or the conditions are no longer favorable.

The experiments at 30 and 40 °C in Fig. 7 indicate, by the disposition of the curves, that the increment in temperature changes significantly the reaction mechanisms: at 30 °C the formation of peak 1 is barely visible regardless the *w/c*, however the appearance of the dormant period is clear and very narrow; for $w/c = 0.5$ the RHL drops almost zero and for $w/c = 0.4$ remains at 6 W/kg before the onset of peak 2, which assumes a very rapid initial dissolution of the CSA clinker and the start of the processes of gypsum formation. Peak 2 is observable at 1.3 h at 30 °C for both *w/c* with a practically nonexistent dormant period, followed almost immediately by peak 3, which in both cases reach a maximum of ~4 h (9.8 W/kg for 415 and 9.7 W/kg for 515) followed by a decrease in the RHL that extends until after 10 h. It is interesting to note the formation of a peak 4 at 17 and 21 h for $w/c = 0.5$ and 0.4 respectively, probably caused by the growth of ettringite crystals. In the experiments at 40 °C, an overlapping of peak 2 and 3 starting at 1 h was observed, indicating that gypsum and ettringite formation were developed into a single step, reaching a maximum of 14.7 and 16.2 W/kg for $w/c = 0.4$ and 0.5 respectively. In this case the apparition of peak 4 is at 11 and 17 h for $w/c = 0.5$ and 0.4 respectively, similar to that observed at 30 °C, indicating that crystal growth is hindered at lower *w/c*.

Figure 8 shows calorimetry curves for pastes with different hemihydrate content. In the three systems it is clear the formation of the first three peaks: increasing the $CaSO_4 \cdot ½H_2O$ content, the maximum RHL for peak 2 increased, while its dormant period appeared earlier and increased in intensity, reaching 0, 0.4 and 0.5 W/kg for 15, 20 and 25 % hemihydrate, respectively, displacing the maximum of peak 3 at earlier times (see vertical lines). This suggests that the higher amount of sulfates in the systems lead to an intense hemihydrate→gypsum conversion that acted as a catalyst for the CSA reactions due to intense heat liberation at short times. It is interesting to note that the

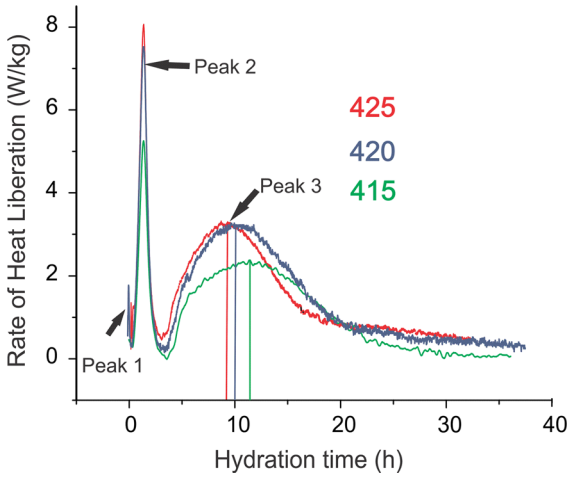

Fig. 8 Isothermal conduction calorimetry for the systems 415, 420 and 425 at 20 °C

total accumulated heat in the analyzed systems was of 250–320 kJ/kg, which is in the permissible range for Portland cements (ASTM- C-150 [32]).

4 Conclusions

- It is feasible the synthesis of calcium sulfoaluminate clinker at 1250 °C using aluminum slag, fly ash and fluorgypsum. Nevertheless, low content of belite and an increased amount of gehlenite was observed.
- The main hydration product was ettringite which showed a needle-like morphology and irregular shaped plates. Presence of $Al(OH)_3$ was also detected; no monosulphate was formed in the hydration products.
- In general, the compressive strength of the pastes at 360 days was of ~40 MPa.
- The setting times were higher with higher *w/c*, and were reduced increasing the amount of hemihydrate by an accelerated formation of ettringite.
- Delayed ettringite formation was responsible for strength drops at 90 days; while at later ages, decreases were caused by the continuous growth of this phase.
- Pastes with higher *w/c* presented lower pH in the curing media due to the differences in the concentration of solids in the paste. Higher content of gypsum led to lower pH attributed to good impermeability and an increased amount of ettringite.
- Isothermal conduction calorimetry showed that the reactions are strongly affected by the temperature, *w/c* and hemihydrate content. Increasing the temperature caused an overlap of gypsum and ettringite formations (peaks 2 and 3).

Acknowledgments SEP-PRODEP: PRODEP DSA/103.5/15/7082 UACOAH-PTC-332, PRODEP DSA/103.5/15/7082 UACOAH-PTC-343. Gallardo-Heredia would like to thank CONACYT for the scholarship granted to develop this research.

Compliance with ethical standards

Conflict of interest The authors declare that they have no conflict of interest.

References

1. Avila-Lopez U, Almanza-Robles JM, Escalante-Garcia JI (2015) Investigation of novel waste glass and limestone binders using statistical methods. Constr Build Mat 82:296–303
2. Escalante JI (2002) Materiales alternativos al cemento Portland. Av Perspect 21:79–88
3. Ramachandran VS (2001) Concrete science. In: Beaudoin JJ (ed) Handbook of analytical techniques in concrete science and technology principles, techniques and applications. Noyes Publications, Norwich, pp 1–55
4. Gartner E (2004) Industrially interesting approaches to "low-CO_2" cements. Cem Concr Res 34:1489–1498. doi:10.1016/j.cemconres.2004.01.021
5. Roszczynialski W, Gawlicki M, Nocun-Wczelik W (1996) Production and use of by-product gypsum in the construction industry. In: Chandra S (ed) Waste materials used in concrete manufacturing. Noyes Publications, Westwood, pp 53–130
6. Hanein T, Imbabi MS, Glasser FP, and Bannerman MN (2016), Lowering the carbon footprint and energy consumption of cement production: A novel Calcium SulfoAluminate cement production process. In proceedings of the 1st International Conference on Grand Challenges in Construction Materials, Los Angeles
7. García-Maté M, De la Torre AG, León-Reina L, Losilla ER, Aranda MAG, Santacruz I (2015) Effect of calcium sulfate source on the hydration of calcium sulfoaluminate eco-cement. Cem Concr Compos 55:53–61. doi:10.1016/j.cemconcomp.2014.08.003
8. Mehta PK, Klein A (1965) Formation of ettringite by hydration of a system containing an anhydrous calcium sulfoaluminate. J Am Ceram Soc 48:435–436. doi:10.1111/j.1151-2916.1965.tb14786.x
9. Sharp JH, Lawrence CE, Yang R (1999) Calcium sulfoaluminate cements—low-energy cements, special cements or what? Adv Cem Res 11:3–13. doi:10.1680/adcr.1999.11.1.3
10. Arjunan P, Silsbee MR, Roy DM (1999) Sulfoaluminate-belite cement from low-calcium fly ash and sulfur-rich and other industrial by-products. Cem Concr Res 29:1305–1311. doi:10.1016/S0008-8846(99)00072-1

11. Katsioti M, Tsakiridis PE, Agatzini-Leonardou S, Oustadakis P (2005) Examination of the jarosite–alunite precipitate addition in the raw meal for the production of Portland and sulfoaluminate-based cement clinkers. Int J Miner Process 76:217–224. doi:10.1016/j.minpro.2005.01.007
12. Li H, Agrawal DK, Cheng J, Silsbee MR (2001) Microwave sintering of sulphoaluminate cement with utility wastes. Cem Concr Res 31:1257–1261. doi:10.1016/S0008-8846(01)00579-8
13. Li J, Ma H, Zhao H (2007) Preparation of sulphoaluminate-alite composite mineralogical phase cement clinker from high alumina fly ash. Key Eng Mater 334–335:421–424. doi:10.4028/www.scientific.net/KEM.334-335.421
14. Murayama N, Maekawa I, Ushiro H, Miyoshi T, Shibata J, Valix M (2012) Synthesis of various layered double hydroxides using aluminum dross generated in aluminum recycling process. Int J Miner Process 110–111:46–52. doi:10.1016/j.minpro.2012.03.011
15. Singh M, Kapur PC (2008) Preparation of calcium sulphoaluminate cement using fertiliser plant wastes. J Hazard Mater 157:106–113. doi:10.1016/j.jhazmat.2007.12.117
16. Singh M, Upadhayay SN, Prasad PM (1997) Preparation of iron rich cements using red mud. Cem Concr Res 27:1037–1046. doi:10.1016/S0008-8846(97)00101-4
17. Ministerio de Medio Ambiente. Lista europea de residuos. MAM, BOE 19/2/2014, Spain
18. Odler I (2000) Special inorganic cements. Taylor and Francis Group, London
19. Kuryatnyk T, Chabannet M, Ambroise Pera J (2008) Improvement of calcium sulphate water resistance by addition of calcium sulphoaluminate clinker clinker. Mater Lett 62:3713–3715. doi:10.1016/j.matlet.2008.04.036
20. Winnefeld F, Lothenbach B (2010) Hydration of calcium sulfoaluminate cements- Experiemntal findings and thermodynamic modelling. Cem Concr Res 40:1239–1247. doi:10.1016/jcemconres.2009.08.014
21. Kalogridis D, Kostogloudis GCh, Ftikos Ch, Malami Ch (2000) A quantitative study of the influence of non-expansive sulfoaluminate cement on the corrosion of steel reinforcement. Cem Concr Res 30:1731–1740. doi:10.1016/S0008-8846(00)00277-5
22. Mehta PK (1967) Expansion characteristics of calcium sulfoaluminate hydrates. J Am Ceram Soc 50:204–208. doi:10.1111/j.1151-2916.1967.tb15082.x
23. Gallardo M, Almanza JM, Cortés DA, Escobedo JC, Escalante-García JI (2014) Synthesis and mechanical properties of a calcium sulphoaluminate cement made of industrial wastes. Mater. Constr 64:e0231–e0238. doi:10.3989/mc.2014.04513
24. Taylor HFW (1997) Cement chemistry, 2nd edn. Thomas Telford edition, Great Britain
25. Chen IA, Hargis CW, Juenger MCG (2012) Understanding expansion in calcium sulfoaluminate-belite cements. Cem Concr Res 42:51–60. doi:10.1016/j.cemconres.2011.07.010
26. Clark BA, Brown W (2000) The formation of calcium sulfoaluminate hydrate compounds Part II. Cem Concr Res 30:233–240. doi:10.1016/S0008-8846(99)00234-3
27. Allevi S, Marchi M, Scotti F, Bertini S, Cosentino C (2015) Hydration of calcium sulphoaluminate clinker with additions of different calcium sulphate sources. Mater Struct 49:453–466. doi:10.1617/s11527-014-0510-5
28. NMX-C-085-ONNCCE-2002. Construction industry – Hydraulic cements – Standard test method for mechanical mixing of hydraulic cement pastes and mortars. ONNCCE, México, D.F.;2002 [In Spanish]
29. ASTM C 20 (2010) Standard test methods for apparent porosity, water absorption, apparent specific gravity, and bulk density of burned refractory brick and shapes by boiling water. ASTM International, West Conshohocken
30. Forrester JA (1970) A conduction calorimeter for two study of cement hydration. Cem Technol 1:95–99
31. ASTM C 150 (2004) Standard specification for portland cement. ASTM International, West Conshohocken
32. NMX-C-061-ONNCCE-2001 (2001) Construction industry-hydraulic cements-determination of compressive strength of hydraulic cements. ONNCCE, [In Spanish]
33. ASTM C 191 (2004) test method for time of setting of hydraulic cement by Vicat. ASTM International, West Conshohocken
34. Sleiman H, Perrot A, Amziane S (2010) A new look at the measurement of cementitious paste setting by Vicat Test. Cem Concr Res 40:681–686. doi:10.1016/j.cemconres.2009.12.001
35. Velazco G, Almanza JM, Cortés DA, Escobedo JC, Escalante-Garcia JI (2014) Effect of strontium aluminate and hemihydrate contents on the properties of a calcium sulphoaluminate based cement. Mater Constr 64(315):e024. doi:10.3989/mc.2014.04413
36. Gallardo-Heredia M (2015) Synthesis and properties of calcium sulphoaluminate cements made from industrial wastes. Ph. D. Thesis, Center of Reseach an Advances Studies (Cinvestav Saltillo), (In Spanish)
37. NMX-C-414-ONNCCE-2004 (2004) Construction industry-hydraulic cements-specifications and testing methods. ONNCCE, [In Spanish]
38. Sánchez-Herrero MJ, Fernández-Jiménez A, Palomo A (2013) C_4A_3S hydration in different alkaline media. Cem Concr Res 46:41–49. doi:10.1016/j.cemconres.2013.01.008
39. Yang H, Jiang L, Zhang Y, Pu Q, Xu Y (2012) Predicting the calcium leaching behavior of cement pastes in aggressive environmets. Constr Build Mater 29(88):96. doi:10.1016/j.conbuildmat.2011.10.031
40. Magallanes-Rivera RX, Escalante-García JI, Gorokhovsky A (2009) Hydration reactions and microstructural characteristics of hemihydrate with citric and malic acid. Constr Build Mater 23:1298–1305. doi:10.1016/j.conbuildmat.2008.07.022
41. Álvarez-Pinazo G, Cuesta A, García-Maté M, Santacruz I, Losilla ER, Sanfélix SG, Fauth F, Aranda MAG, De la Torre AG (2014) In-situ early-age hydration study of sulfobelite cements by synchrotron powder diffraction. Cem Concr Res 56:112–119. doi:10.1016/j.cemconres.2013.10.009
42. Taylor HFW, Famy C, Scrivener KL (2001) Delayed ettringite formation. Cem Concr Res 31:683–693. doi:10.1016/S0008-8846(01)00466-5
43. Escalante-García JI, Rios-Escobar M, Gorokhovsky A, Fuentes AF (2008) Fluorgypsum binders with OPC and PFA additions, strength and reactivity as a function of component proportioning and temperature. Cem Concr Compos 30(2):88–96